P1M.12 RELATIONSHIPS BETWEEN MIXED-PHASE MICROPHYSICAL COLLECTION AND MODELED PRECIPITATION IN VARIOUS REGIMES

Brian J. Gaudet and Elizabeth A. Ritchie *
University of New Mexico, Albuquerque, New Mexico.

1. INTRODUCTION

Accurate precipitation forecasts is a perennial problem in numerical weather forecasting, necessitating the use of an appropriate cloud microphysics scheme (Thompson et al. 2004). Furthermore, recent modeling studies have indicated the sensitivity to microphysical parameters of details of storm structure (Wakimoto et al. 2004; van den Heever and Cotton 2004; Gilmore et al. 2004b) and even prototype Doppler retrievals of temperature fields (Dowell et al. 2004).

In this abstract we focus on one diagnosed potential problem of the standard treatment of hydrometeor collection in microphysics scheme. Using the Coupled Ocean/Atmosphere Mesoscale Prediction System (COAMPS), we implement a microphysics scheme where the diagnosed problem is corrected. Though we only consider the COAMPS microphysics here, the issues discussed have general applicability to other schemes. Sensitivity tests between the standard and modified scheme are performed on an idealized case involving the transformation of a tropical cyclone remnant into an extratropical system. This scenario exhibits both warm-rain and cold-rain microphysics, depending on simulation time. After describing the model setup, we discuss the modified microphysics, and then present the model comparison tests. We then conclude and mention possibilities for future work.

2. MODEL AND SIMULATION OVERVIEW

COAMPS® is a non-hydrostatic three-dimensional compressible model developed by the Naval Research Laboratory in Monterey, CA. More information about the model can be found in Hodur (1997). The standard microphysics scheme is based on the single moment bulk method found in Rutledge and Hobbs (1983, 1984); the mixing ratios of cloud water, rain, pristine ice, snow, and graupel are predicted. For all simulations presented here the microphysics was modified so that hydrometeor collection is calculated through the use of numerical integration and lookup tables, to avoid the biases associated with approximate forms of the collection integral (see for example Gaudet and Schmidt 2005a).

The simulations were performed in an idealized framework. The tropical/extratropical cyclone simulations used an initial condition consisting of the superposition of an idealized upper-level trough and a tropical cyclone, as described in Ritchie and Elsberry (2003) (see Figure 1). The simulation consists of a single grid, 319×337, with 27 km horizontal spacing. There is no surface topography in the simulation (political boundaries are left in the figures for spatial reference). Timesteps of both 60 s and 20 s are used.

During the simulation the tropical cyclone weakens and progresses northward, approaching a baroclinic zone forming in advance of the midlevel trough by 36 h (Figure 2). Around 50 h, the minimum central pressure stops increasing and the tropical cyclone remnant begins to interact with the trough. By 60 h the two are no longer distinguishable at 500 mb. At this time significant concentrations of ice-phase hydrometeors appear along the baroclinic zone, so we will focus most of the analysis on this period.

3. THEORETICAL CONCEPT

In a bulk microphysics model the total mass content (mass of hydrometeor per unit volume) of a species x can be expressed as $\int X(D)dD$ where D is diameter and $X(D) = m(D)n(D)$ is the product of the mass of a hydrometeor of size D and its number concentration density between D and $D + dD$. If species x is being collected, the mass content depletion is generally discretized as $\Delta t \int (dX/dt)dD$, where Δt is the timestep, and:

$$\frac{dX}{dt} = -X\lambda,$$

$$\lambda \equiv \int \pi \frac{(D_x + D_y)^2}{4} |v_x(D_x) - v_y(D_y)| n_y(D_y) dD_y, \quad (1)$$

where $v(D)$ is the terminal fall velocity, and y denotes the collector species. A problem with (1) is that if $\lambda \Delta t$ exceeds unity, so will the normal discretized fractional depletion of X, necessitating *ad hoc* renormalizations. One solution (Gaudet and Schmidt 2005b) is to basically solve the differential equation in (1), assuming that λ stays roughly constant during the timestep. This gives $X = X_0 e^{-\lambda \Delta t}$, where X_0 is the mass content at the beginning of the timestep, and so the corrected depletion of x is given by:

$$\int (X - X_0) dD_x = -\int [1 - e^{-\lambda \Delta t}] X_0 dD_x. \quad (2)$$

This quantity is assured to be no greater than the initial mass content, regardless of timestep. The use of the bracketed term in (2) was referred to in Gaudet and

*Corresponding author address: Brian J. Gaudet, Department of Electrical and Computer Engineering, 1 University of New Mexico, Albuquerque, NM 87131; e-mail: bgaudet@ece.unm.edu.

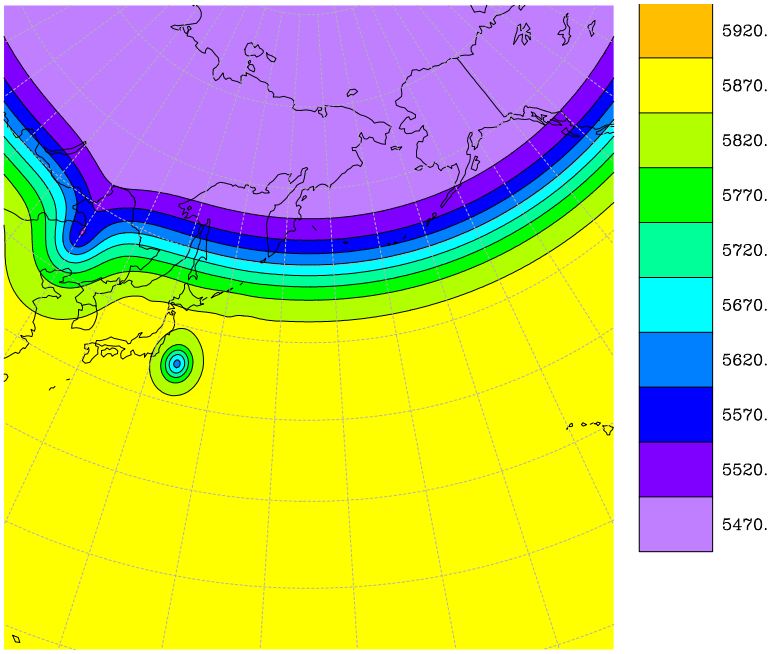

Figure 1: Geopotential heights (m) at 500 mb for model initialization.

Schmidt (2005b) as numerical bounding, and is a continuous version of the collection-limiting procedure of Ferrier (1994). (It can also be related to the Poisson discrete model of Young (1975).) As Δt is reduced, the difference between the bounded and unbounded solution goes to zero.

This can be generalized to the case of more than one species collecting x simultaneously. If x is being collected by y and z, we have, for each size bin of x:

$$\frac{dX}{dt} = -X\lambda_y - X\lambda_z$$

$$\frac{dY}{dt} = X\lambda_y$$

$$\frac{dZ}{dt} = X\lambda_z. \qquad (3)$$

The solution is $X = X_0 e^{-(\lambda_y+\lambda_z)\Delta t}$, $Y = Y_0 + (\lambda_y/(\lambda_y + \lambda_z))X_0(1 - e^{-(\lambda_y+\lambda_z)\Delta t})$, and $Z = Z_0 + (\lambda_z/(\lambda_y + \lambda_z))X_0(1 - e^{-(\lambda_y+\lambda_z)\Delta t})$. Integrating over D_x, we see that the λ in (2) becomes the sum of the λ for all of the collection processes, and each collection pathway i receives a fraction $\lambda_i / \sum \lambda_i$ of the total amount collected from each size bin $(D_x, D_x + dD_x)$.

For the COAMPS standard microphysics, the hydrometeor collection interactions considered are rain collecting snow, snow collecting rain, graupel collecting snow, and graupel collecting rain. In the absence of melting or shedding, and provided hydrometeor amounts exceed certain thresholds, the destination category for all these interactions is graupel.

4. SIMULATED MICROPHYSICS COMPARISONS

We now present comparisons between bounded and non-bounded microphysics in numerical simulations of the extratropical transition case using COAMPS. Figure 3 shows the graupel mixing ratio for the stratiform precipitation region of the baroclinic zone at 60 h of simulation time and 600 mb, which is slightly above the freezing level. A 60 s timestep was used. A comparison with the unbounded solution (Figure 4) shows approximately 30% more graupel in the latter. In contrast, about 25% more snow is present in the bounded solution (Figure 5) versus the unbounded solution (Figure 6). Since the default destination class of all collection interactions is graupel, the results are consistent with what would be expected.

We now compare the same simulations, but using a 20 s timestep. As expected, the difference between the bounded and unbounded solutions are much reduced (Figures 7 - 10). For both snow and graupel, the reduced timestep cases show more resemblance to the 60 s bounded case than to the 60 s unbounded case. In the case of snow the resemblance between the 20 s solutions and 60 s bounded solution is quite close. However, though the 60 s bounded graupel maximum is not as large as the 60 s unbounded graupel maximum, it is still significantly larger than either 20 s graupel maxima, suggesting that the bounded microphysics still has timestep sensitivities.

For rain, there is little discernible difference at 600 mb and 60 h between the bounded and unbounded $\Delta t = 60$ s simulations (not shown), and no systematic trend

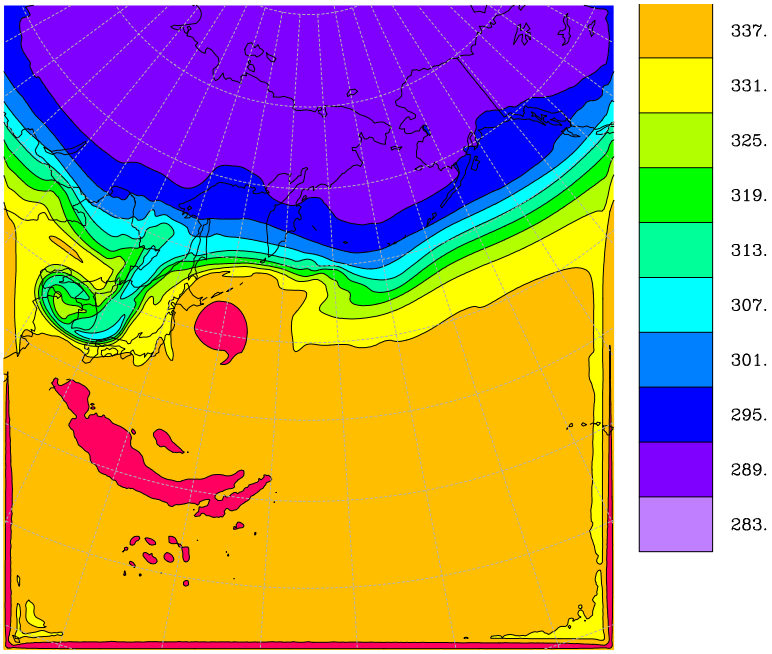

Figure 2: Equivalent potential temperature (K) at 850 mb for 36 h of simulation time.

throughout the simulation. At 700 mb (below the freezing level) the unbounded simulation produces slightly more rain, evidently due to the melting of more graupel (Figures 11 and 12). However, both bounded and unbounded rain fields contain considerable more rain mixing ratio than either 20 s simulation (Figures 13 and 14).

In the 36-60 h time frame, the 700 mb rain fields are quite similar between the bounded and unbounded simulations (not shown). Even more so than at 60 h, the difference between $\Delta t = 60$ s and $\Delta t = 20$ s is much greater than between bounded and unbounded, with the $\Delta t = 60$ s simulations producing much greater amounts of mixing ratio along the baroclinic zone at 36 h (Figures 15 and 16). In general, the 20 s accumulated precipitation fields are smoother (Figures 17 and 18).

As previously mentioned, before 60 h the mixing ratios of ice hydrometeors are significantly lower along the baroclinic zone, thus accounting for the decreased significance of numerical bounding. Of course, in warm-phase precipitation processes the only species are rain and cloud water, whose interaction is not involved in the above formulation. As expected, during the early stages of the simulation, when warm rain from the tropical cyclone is dominant, numerical bounding makes little difference. However, the sensitivity of precipitation to model timestep becomes even more apparent, in part because of the greater precipitation rates (Figures 19 and 20). For the 20 s timestep, the precipitation amounts are greater.

5. DISCUSSION

The following conditions make it more likely that the use of numerical bounding will have a significant effect: 1) the timesteps should be of the order of 50 s or greater (i.e., relatively large scale simulations), and 2) the amounts of both liquid and ice hydrometeors should be large in subfreezing temperatures. These conditions may be most likely in vigorous synoptic extratropical stratiform precipitation, or possibly the stratiform regions of MCSs.

For extremely large hydrometeor mixing ratios (e.g., in certain supercells), it is possible that numerical bounding may make little difference in a single moment scheme, because by any method essentially all of the mixing ratio of the collected species is depleted. But in these cases numerical bounding may become important when multi-moment or bin microphysics are used, because it limits the collected mass for each size bin of collected hydrometeor, whereas standard methods simply limit the total mass (or other integrated moment) collected. Thus the use of numerical bounding can provide more information about the evolution of distributions during collection.

Clearly, the simulation of a case study is needed to provide observational support as to which method provides 'better' results. It is also clear that there are more issues with regard to simulated precipitation and hydrometeor fields than overcollection. The great sensitivity of these to model timestep warrants further investigation of the timescale assumptions inherent in whole microphysics packages. Furthermore, the change in structure of precipitation patterns with changing timestep suggests that there may be a sensitivity of dynamics to timestep

that is also important to hydrometeor distribution.

6. CONCLUSION

We found that the use of numerical bounding did have a discernible effect on the hydrometeor patterns of an extratropical system, and one that was consistent with the theoretical predictions. However, the effect was rather small in these simulations. Future work could involve evaluating simulations of large-scale, cold-cloud, stratiform precipitation systems, where the numerical bounding effect should be largest. Other sensitivities of microphysics schemes to model timesteps should also be studied.

7. ACKNOWLEDGMENTS

This research was performed under grant #N00014-03-1-0831 of the Office of Naval Research Marine Meteorology Program.

REFERENCES

Dowell, D.C., F. Zhang, L.J. Wicker, C. Snyder, and N.A. Crook, 2004: Wind and temperature retrievals in the 17 May 1981 Arcadia, Oklahoma, supercell: Ensemble Kalman filter experiments. *Mon. Wea. Rev.*, **132**, 1982-2005.

Ferrier, B.S., 1994: A double-moment multiple-phase 4-class bulk ice scheme. 1. Description. *J. Atmos. Sci.*, **51**, 249-280.

Gaudet, B.J., and J.M. Schmidt, 2005a: Assessment of hydrometeor collection rates from exact and approximate equations. Part I: A new approximate scheme. *J. Atmos. Sci.*, **62**, 143-159.

Gaudet, B.J., and J.M. Schmidt, 2005b: Assessment of hydrometeor collection rates from exact and approximate equations. Part II: Numerical bounding. Submitted to *J. Appl. Met.*.

Gilmore, M.S., J.M. Straka, and E.N. Rasmussen, 2004b: Precipitation uncertainty due to variations in precipitation particle parameters within a simple microphysics scheme. *Mon. Wea. Rev.*, **132**, 2610-2627.

Hodur, R.M, 1997: The Naval Research Laboratory's Coupled Ocean/Atmosphere Mesoscale Prediction System (COAMPS). *Mon. Wea. Rev.*, **125**, 1414-1430.

Ritchie, E.A., and R.L. Elsberry, 2003: Simulations of the extratropical transition of tropical cyclones: Contributions by the midlatitude upper-level trough to reintensification. *Mon. Wea. Rev.*, **131**, 2112-2128.

Rutledge, S.A., and P.V. Hobbs, 1983: The mesoscale and microscale structure of organization of clouds and precipitation in midlatitude cyclones. VIII: A model for the "seeder-feeder" process in warm-frontal rainbands. *J. Atmos. Sci.*, **40**, 1185-1206.

Rutledge, S.A., and P.V. Hobbs, 1984: The mesoscale and microscale structure of organization of clouds and precipitation in midlatitude cyclones. XII: A diagnostic modeling study of precipitation development in narrow cold-frontal rainbands. *J. Atmos. Sci.*, **41**, 2949-2972.

Thompson, G., R.M. Rasmussen, and K. Manning, 2004: Explicit forecasts of winter precipitation using an improved bulk microphysics scheme. Part I: Description and sensitivity analysis. *Mon. Wea. Rev.*, **132**, 519-542.

van den Heever, S.C., and W.R. Cotton, 2004: The impact of hail size on simulated supercell storms. *J. Atmos. Sci.*, **61**, 1596-1609.

Wakimoto, R.M., H.V. Murphey, R.G. Fovell, and W.-C. Lee, 2004: Mantle echoes associated with deep convection: Observations and numerical simulations. *Mon. Wea. Rev.*, **132**, 1701-1720.

Young, K.C., 1975: The evolution of drop spectra due to condensation, coalescence and breakup. *J. Atmos. Sci.*, **32**, 965-973.

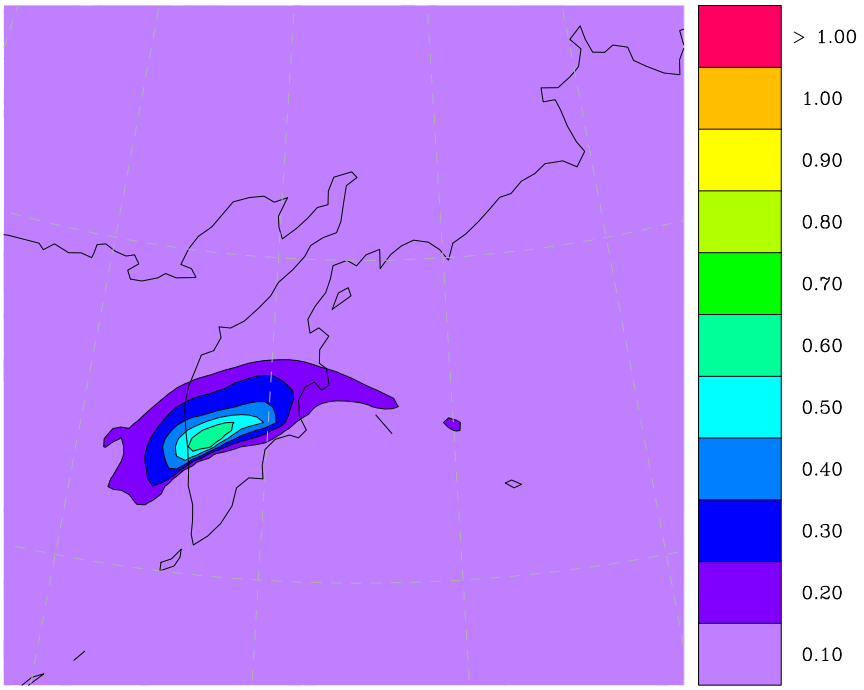

Figure 3: Graupel mixing ratio (g kg^{-1}) for bounded microphysics extratropical cyclone simulation. Pressure is 600 mb, simulation time is 60 h, and timestep is 60 s.

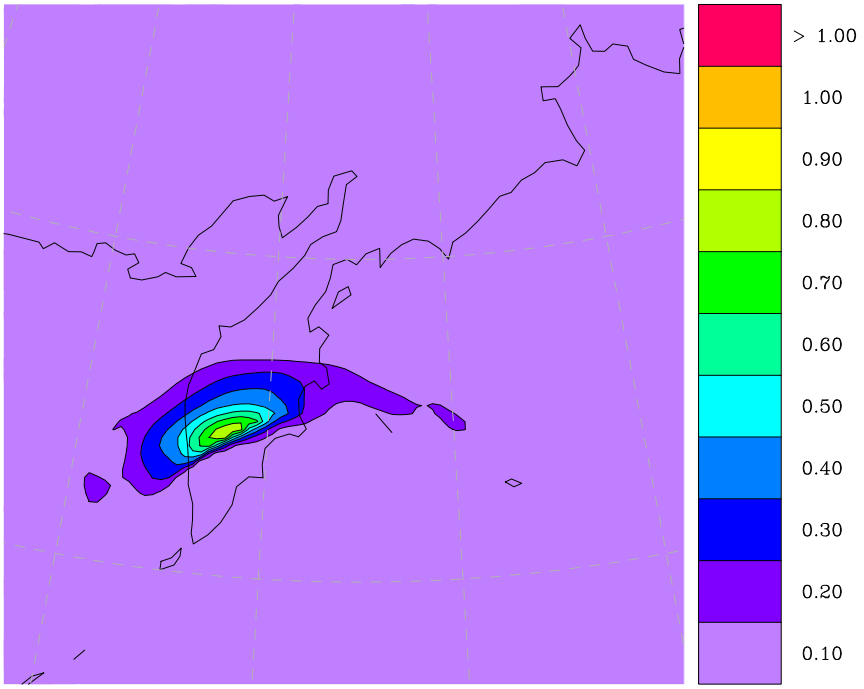

Figure 4: Same as Figure 3, but for unbounded microphysics simulation.

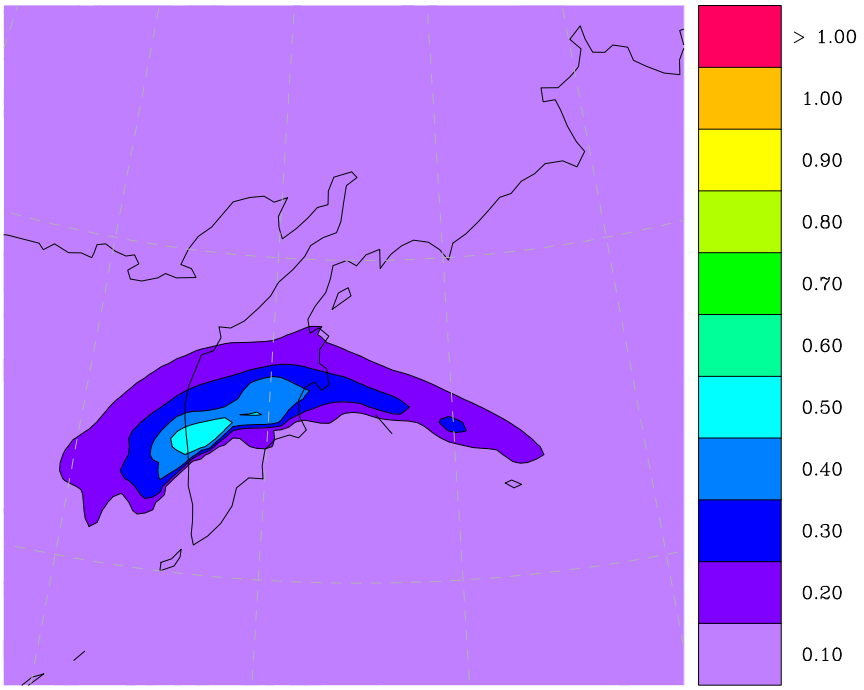

Figure 5: Snow mixing ratio (g kg^{-1}) for bounded microphysics extratropical cyclone simulation. Pressure is 600 mb, simulation time is 60 h, and timestep is 60 s.

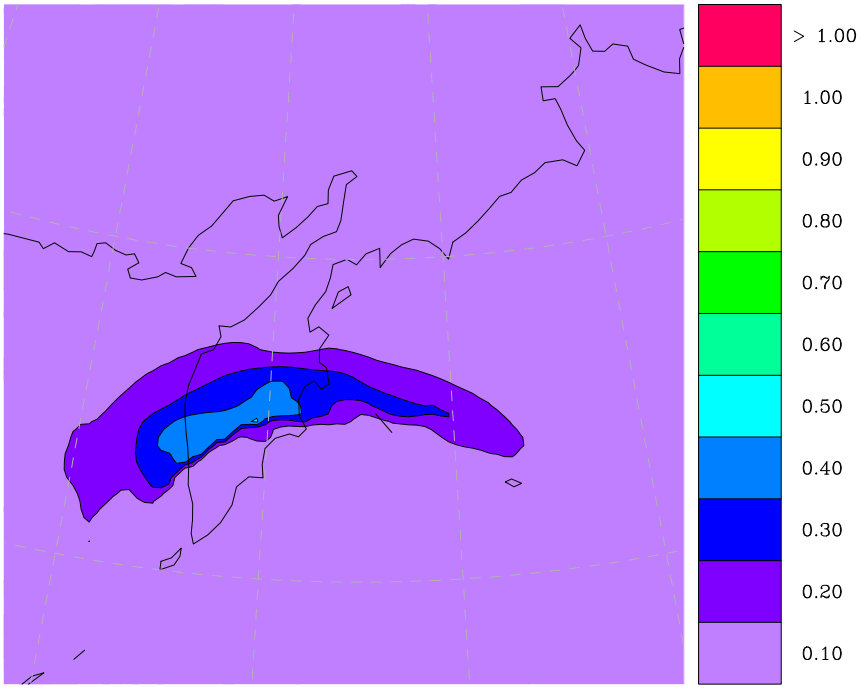

Figure 6: Same as Figure 5, but for unbounded microphysics simulation.

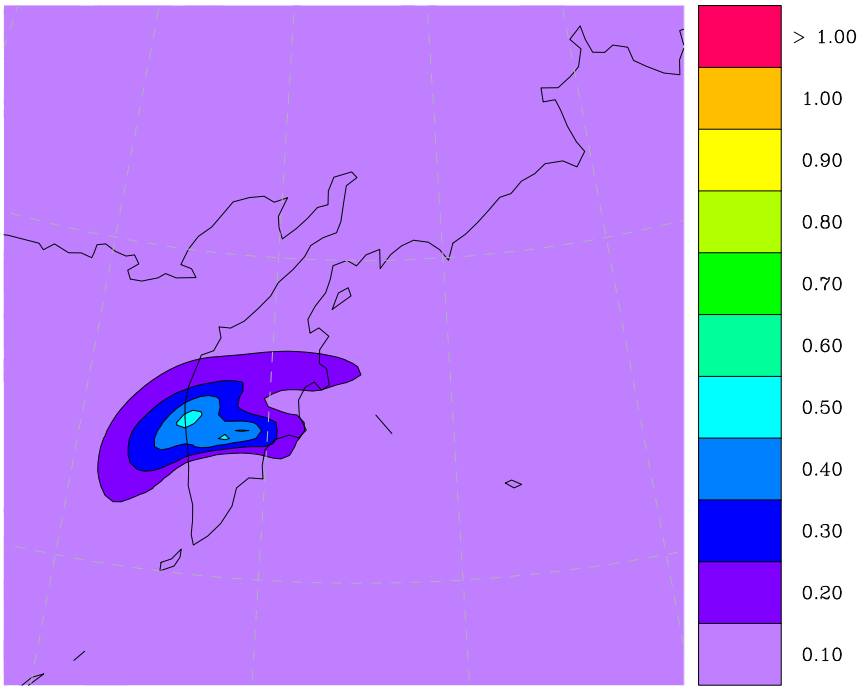

Figure 7: Same as Figure 3, but with 20 s timestep.

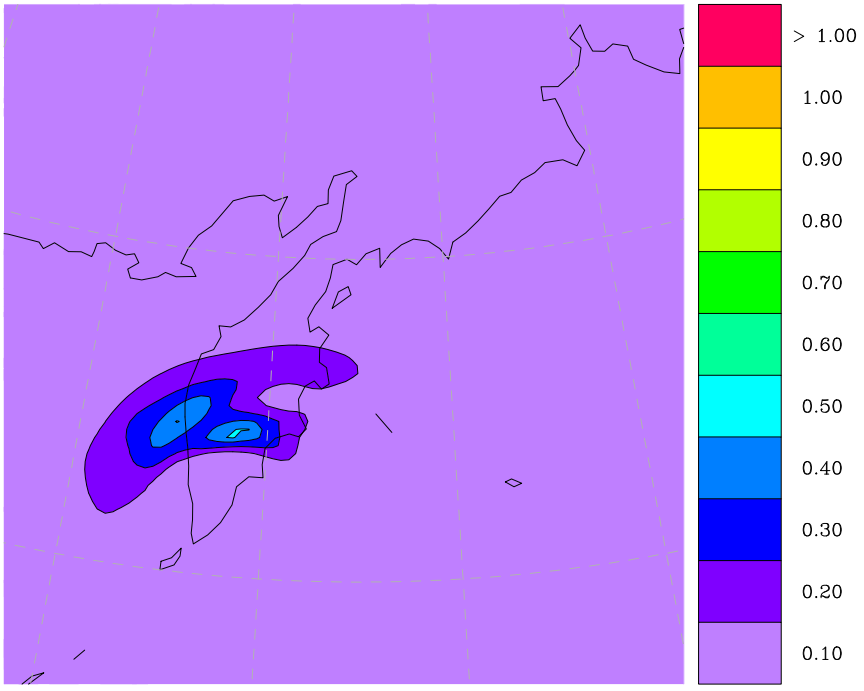

Figure 8: Same as Figure 4, but with 20 s timestep.

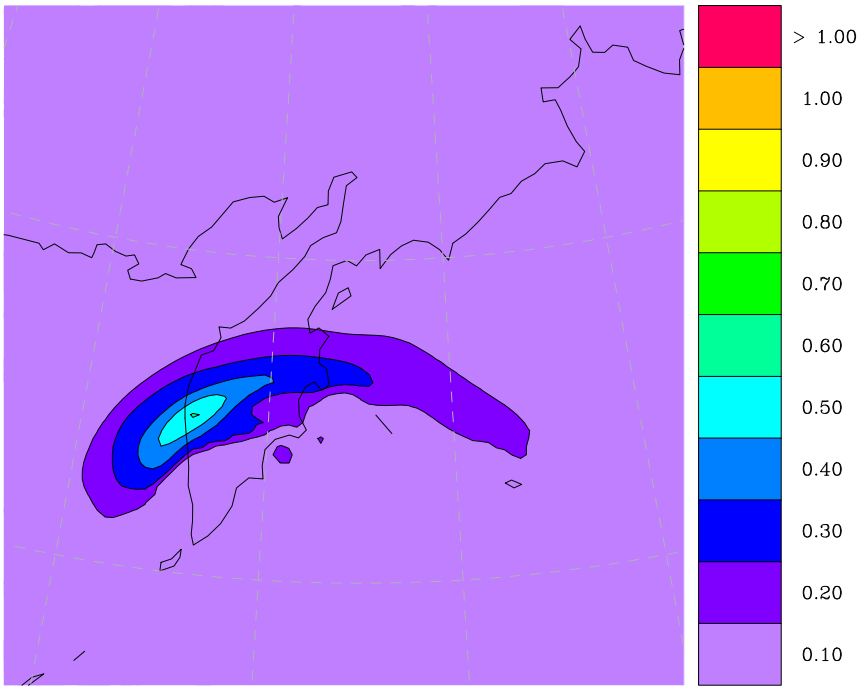

Figure 9: Same as Figure 5, but with 20 s timestep.

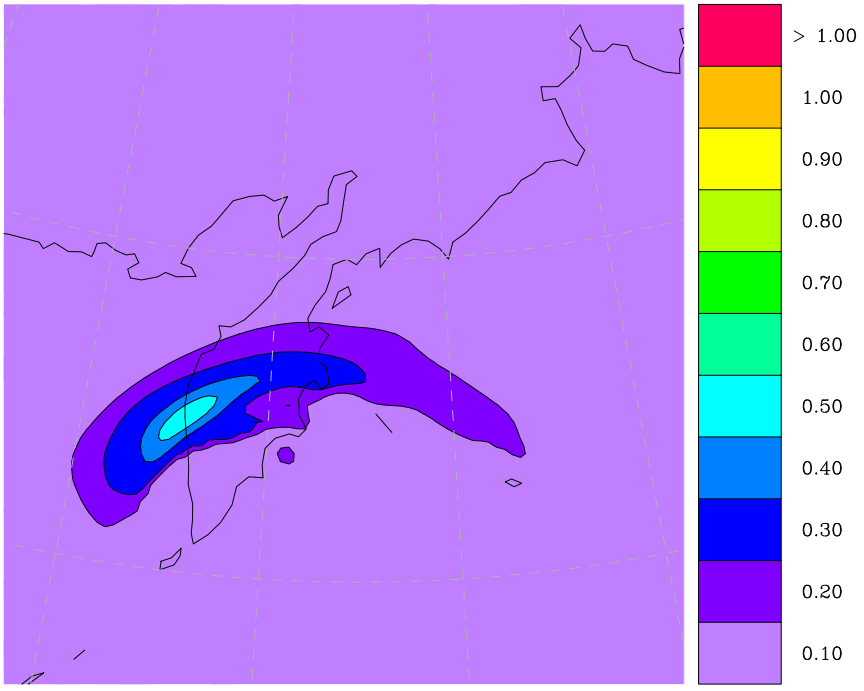

Figure 10: Same as Figure 6, but with 20 s timestep.

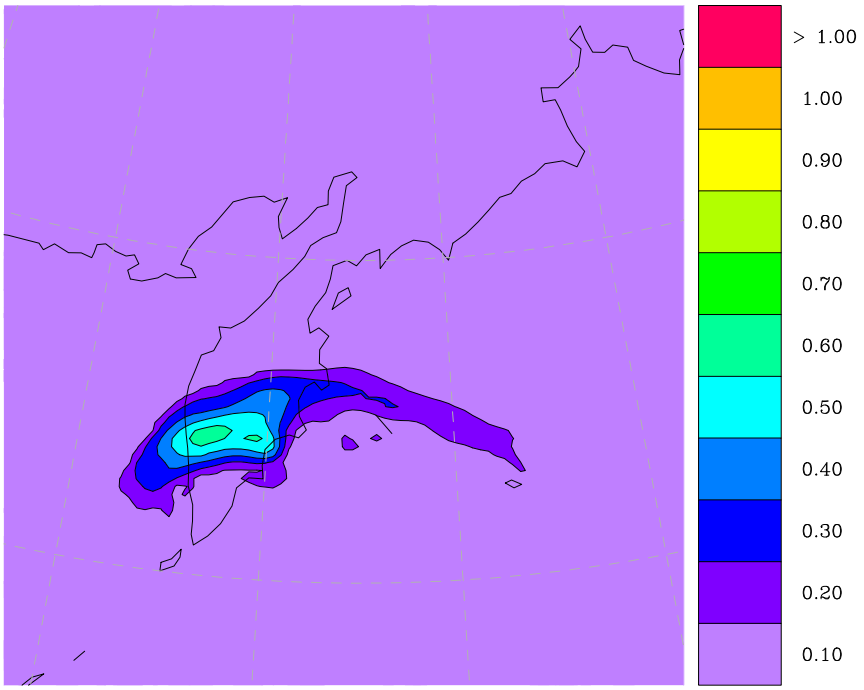

Figure 11: Rain mixing ratio (g kg^{-1}) for bounded microphysics extratropical cyclone simulation. Pressure is 700 mb, simulation time is 60 h, and timestep is 60 s.

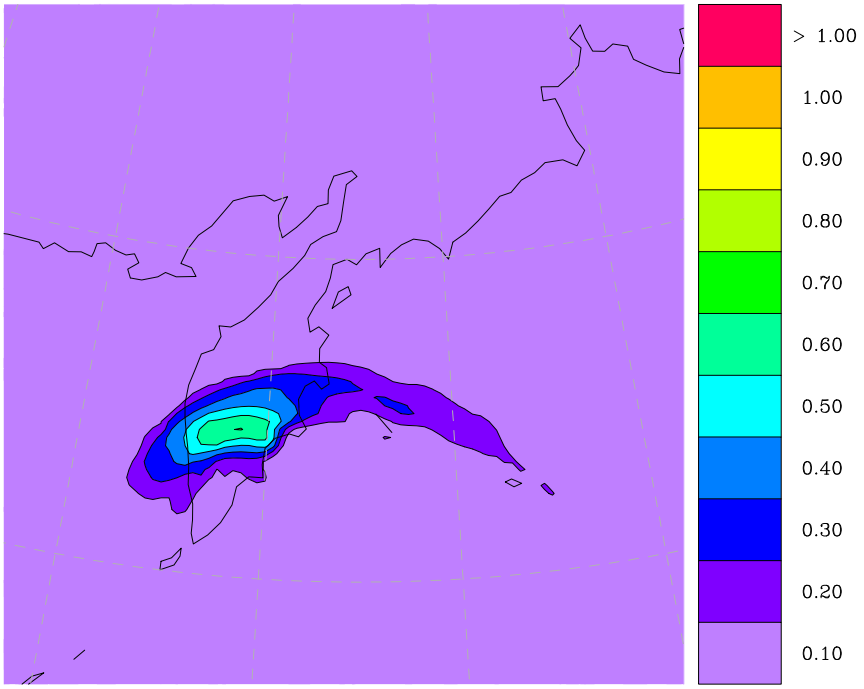

Figure 12: Same as Figure 11, but for unbounded microphysics simulation.

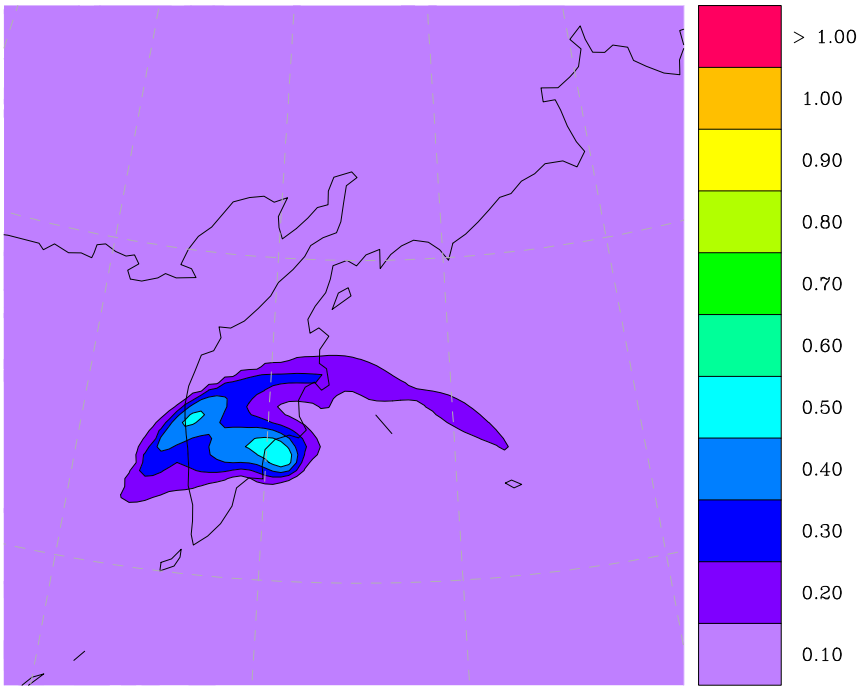

Figure 13: Same as Figure 11, but for 20 s timestep.

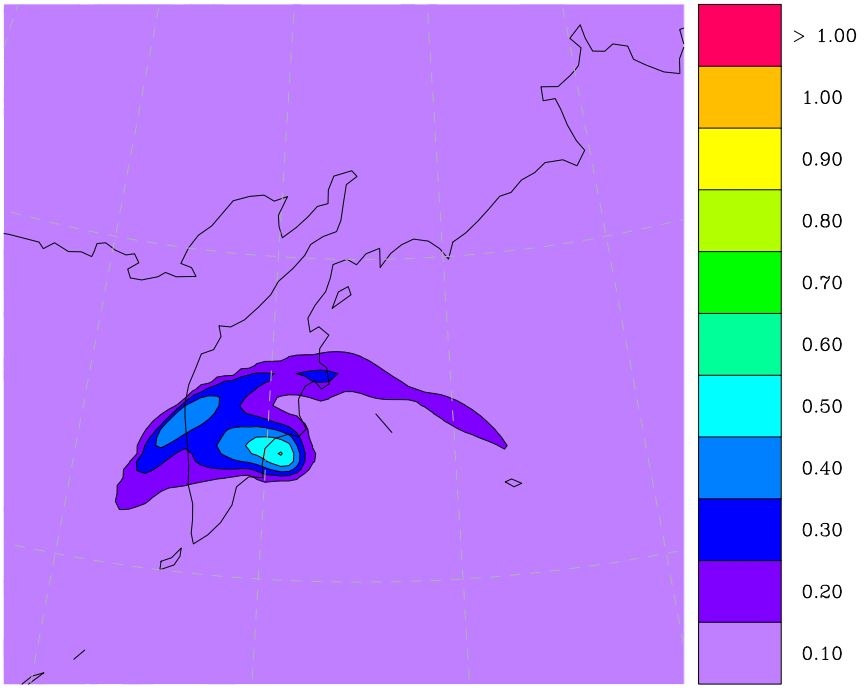

Figure 14: Same as Figure 12, but for 20 s timestep.

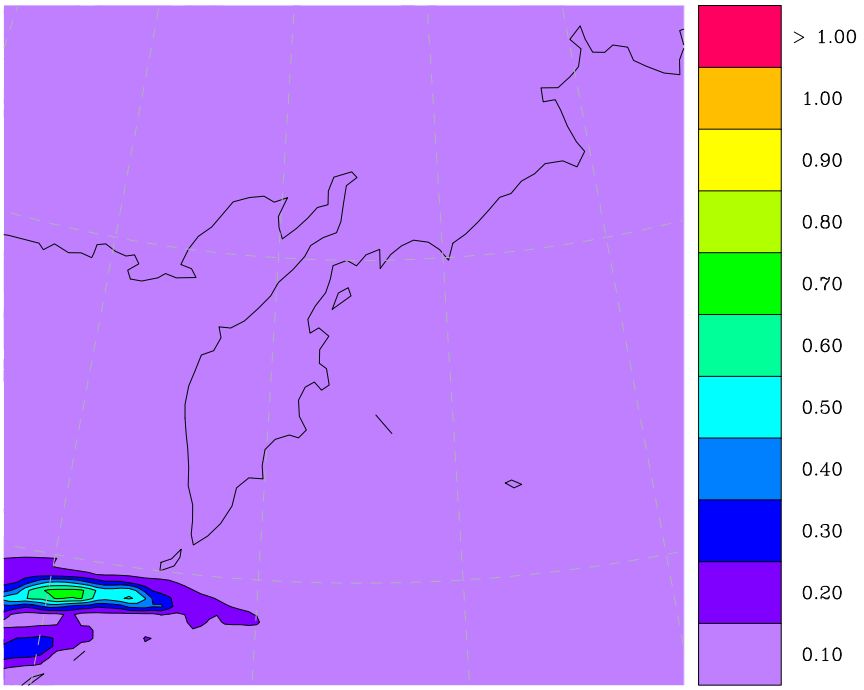

Figure 15: Rain mixing ratio (g kg^{-1}) for bounded microphysics simulation. Pressure is 700 mb, simulation time is 36 h, and timestep is 60 s.

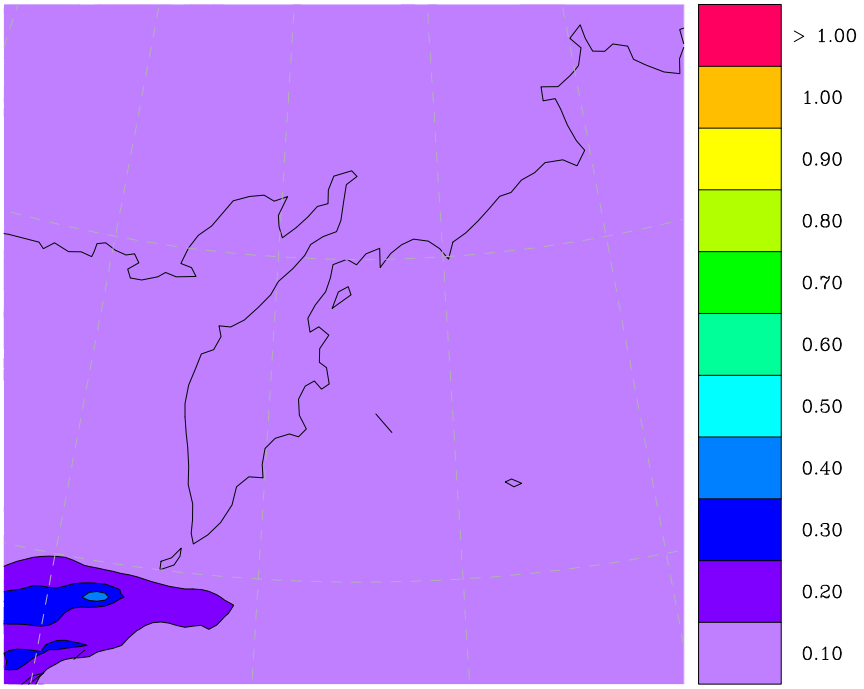

Figure 16: Same as Figure 15, but for 20 s timestep.

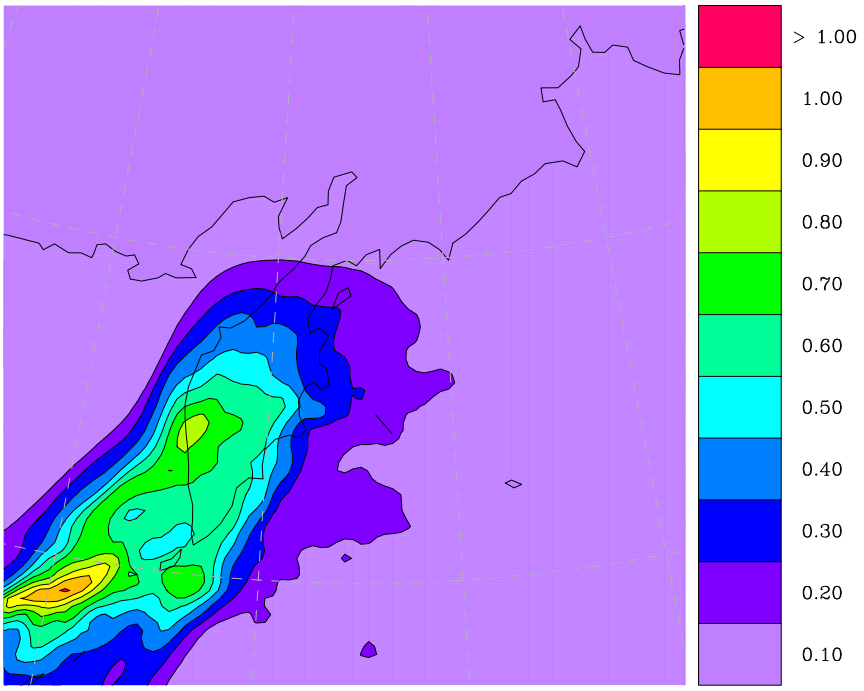

Figure 17: Total model accumulated precipitation (mm) by 72 h for bounded microphysics simulation. Timestep is 60 s.

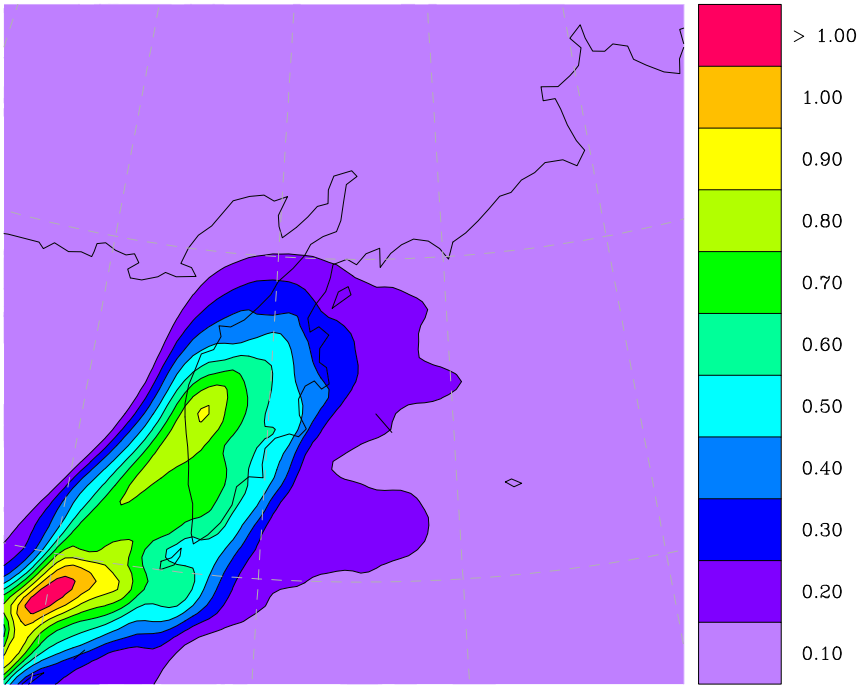

Figure 18: Same as Figure 17, but for 20 s timestep.

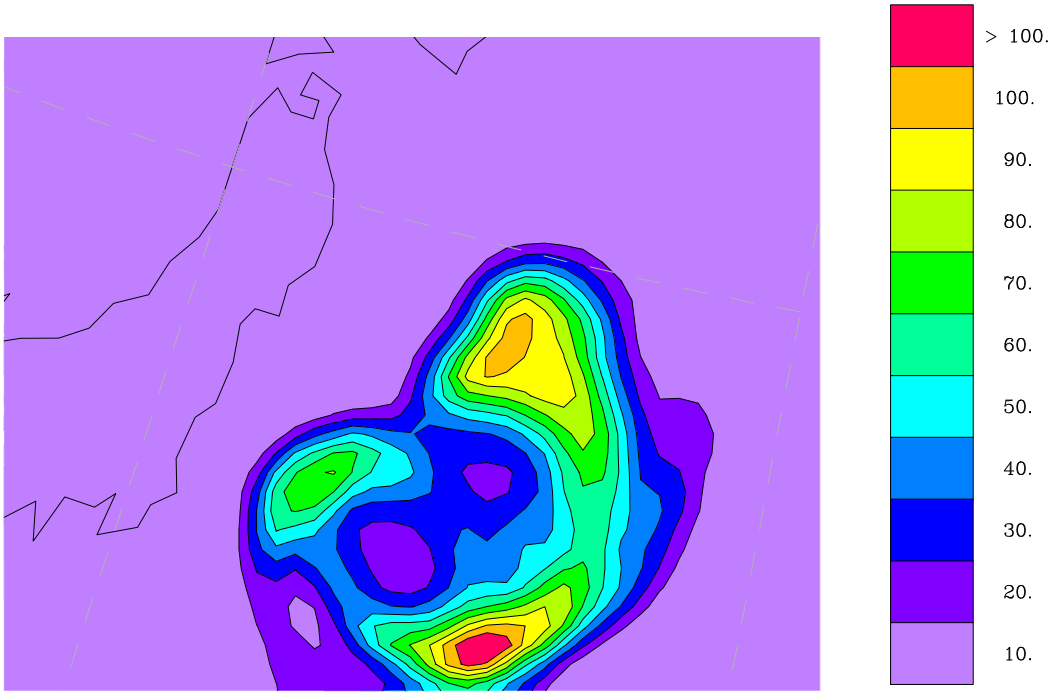

Figure 19: Total model accumulated precipitation (mm) by 24 h for unbounded microphysics simulation. Timestep is 60 s.

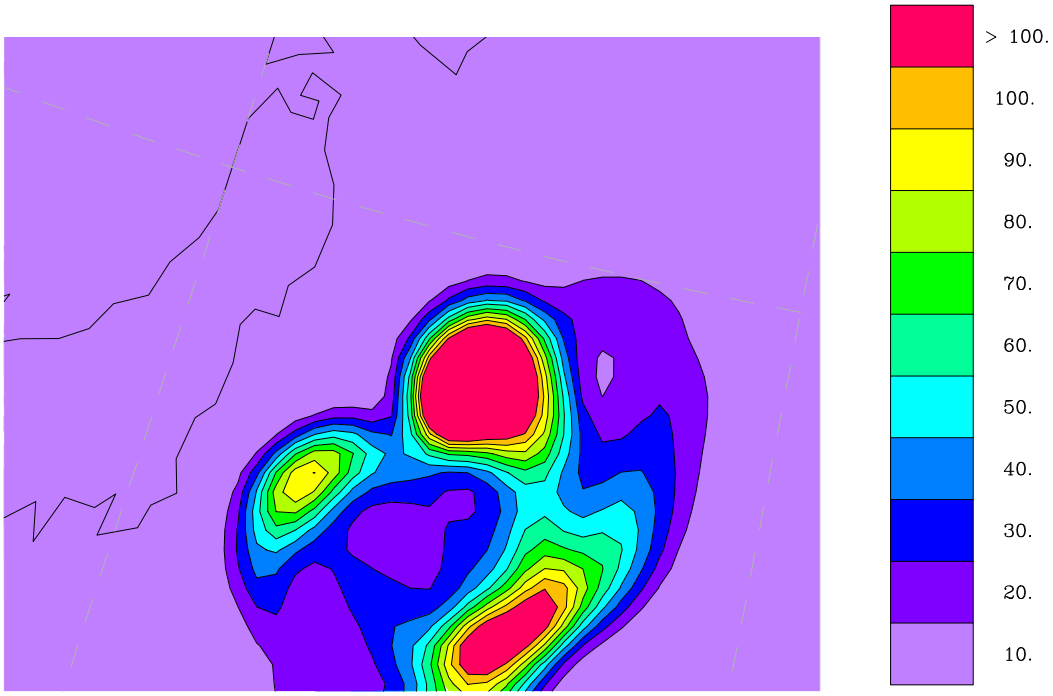

Figure 20: Same as Figure 19, but for 20 s timestep.